Materials Advances

ROYAL SOCIETY OF CHEMISTRY

PAPER

View Article Online
View Journal | View Issue

Cite this: *Mater. Adv.*, 2024, 5, 3058

Synthesis, characterization, and magnetic and antibacterial properties of a novel iron(III) complex $(CH_3)_2NH_2[Fe(phen)Cl_4]$†

Asmae Ben Abdelhadi, [ab] Sara Rodríguez-Sánchez, [c] Rachid Ouarsal, [a] Mohamed Saadi, [d] Lahcen El Ammari, [d] Nicola Morley, [e] Brahim El Bali, [f] Óscar Gómez-Torres, [g] Mohammed Lachkar *[a] and Abderrazzak Douhal *[b]

A novel iron(III) complex $(CH_3)_2NH_2[Fe(phen)Cl_4]$ (**1**) (phen = 1,10-phenanthroline) was synthesized, its structure was fully characterized using different techniques, and its *in vitro* antibacterial activity against various antibiotic-resistant Gram-positive and Gram-negative bacteria was evaluated. The structure of **1** is made up of mononuclear $[Fe(phen)Cl_4]^-$ anions and dimethylammonium cations $(CH_3)_2NH_2^+$. Iron(III) is hexacoordinated to two nitrogen atoms of chelating phenanthroline and four chlorides forming a distorted octahedral environment around the metal atom. Complex **1** crystallizes in a triclinic system with the $P\bar{1}$ space group. 3D Hirshfeld surfaces and 2D fingerprint plots show that H···Cl interactions are the major contributors in maintaining the total surface. IR and UV-visible spectra indicated the coordination of 1,10-phenanthroline to iron (III) metal. Thermal stability experiments revealed that **1** is stable up to 428 K. Magnetic susceptibility measurements indicated a paramagnetic behavior at high temperatures. *In vitro* antibacterial activity was explored against two Gram-positive bacteria, *Staphylococcus aureus* CECT 86 and *Listeria monocytogenes* CECT 4031, and two Gram-negative bacteria, *Escherichia coli* CECT 99 and *Klebsiella pneumoniae* CECT 143T, using the disc diffusion method. Complex **1** clearly showed good activity against these bacteria and is a potential candidate for treating bacterial infections and promoting further development in their treatment.

Received 6th November 2023,
Accepted 14th February 2024

DOI: 10.1039/d3ma00971h

rsc.li/materials-advances

1. Introduction

The intensive use of antibiotics has led to a rapid increase in the multidrug-resistant bacteria that are resistant towards commercially available drugs.[1–3] To overcome the alarming problem of antimicrobial resistance (AMR) to antibiotics,[4,5] the search for new antibiotics and other antimicrobials continues to be an urgent need to combat AMR pathogens. Transition metal complexes are of significant importance owing to their antimicrobial and anticancer activities[6–8] and are sometimes more effective than free ligands.[9,10] In addition, many drugs such as antibiotics possess better pharmaceutical properties when they are in the form of metal transition complexes.[11–13] From this perspective, the synthesis and characterization of new metal complexes and the evaluation of their antibacterial activities have been considered by the global community as part of the solution to overcome AMR.[14,15] Transition metal complexes with 1,10-phenanthroline ligands are of much interest since they display a wide variety of applications in organometallic chemistry, catalysis, electrochemistry, ring-opening metathesis polymerization and biochemistry.[16–20] 1,10-Phenanthroline has a rigid framework and possesses a superb ability to coordinate with many metal ions,[21–25] strong absorption in the ultraviolet spectral region, bright light-emission, and good electroactive and photoactive properties, thus showing potential for technological applications.[26–30] The photochemical and redox properties of complexes can be systematically varied through appropriate substitution on phenanthroline rings.[31–33]

[a] *Engineering Laboratory of Organometallic, Molecular Materials, and Environment (LIMOME), Faculty of Sciences, Sidi Mohamed Ben Abdellah University, 30000 Fez, Morocco. E-mail: mohammed.lachkar@usmba.ac.ma*
[b] *Departamento de Química Física, Facultad de Ciencias Ambientales y Bioquímica, y INAMOL, Campus Tecnológico de Toledo, Universidad de Castilla-La Mancha (UCLM), Avenida Carlos III, S.N., 45071 Toledo, Spain. E-mail: abderrazzak.douhal@uclm.es*
[c] *Departamento de Química Analítica y Tecnología de los Alimentos, Facultad de Ciencias Ambientales y Bioquímica, Universidad de Castilla-La Mancha, Toledo, Spain*
[d] *Laboratoire de Chimie Appliquée des Matériaux, Centre des Sciences des Matériaux, Faculty of Science, Mohammed V University in Rabat, Avenue Ibn Battouta, BP 1014, Rabat, Morocco*
[e] *Department of Materials Science and Engineering, University of Sheffield, Sheffield S1 3JD, UK*
[f] *Independent Scientist, Marrakech, Morocco*
[g] *Facultad de Ciencias Ambientales y Bioquímica, Universidad de Castilla-La Mancha, Toledo, Spain*

† Electronic supplementary information (ESI) available. CCDC 2281265. For ESI and crystallographic data in CIF or other electronic format see DOI: https://doi.org/10.1039/d3ma00971h

Research concerning the coordination chemistry of Fe(III) has intensified in recent years considering its important role in several chemical and biological systems.[34–37] Structural models for the active sites of various iron-containing enzymes have added a wealth of knowledge to our understanding of various aspects of iron chemistry with respect to structural, electrochemical, and magnetic properties.[38,39] The products formed by the reaction of iron(III) chloride with 1,10-phenanthroline as a bidentate nitrogen donor have been widely studied.[40–45] However, only a few of the resulting compounds such as $[FeCl_3(phen)X]$ (X = CH_3OH, H_2O, or Cl),[46] $[Fe(phen)Cl_3(DMSO)]$,[47] $[Fe(phen)_2Cl_2]NO_3$[48] and $[Fe(phen)Cl_3(CH_3OH)]\cdot CH_3OH$[44] have been fully characterized. Herein, we report a novel iron(III) complex with the formula $(CH_3)_2NH_2[Fe(phen)Cl_4]$, termed as **1**, along with its structural characterization as well as spectroscopic, thermal and magnetic properties. Its *in vitro* antibacterial activity was explored and demonstrated against two Gram-positive (*Staphylococcus* (*S.*) *aureus* CECT 86 and *Listeria* (*L.*) *monocytogenes* CECT 4031) and two Gram-negative (*Escherichia* (*E.*) *coli* CECT 99 and *Klebsiella* (*K.*) *pneumoniae* CECT 143T) bacteria using the disc diffusion method.

2. Experimental section

The chemicals used in the synthesis of **1** and characterisation data are described in detail in ESI† as part 1, including elemental analysis for C, H, N and Fe, single and powder crystal X-ray crystallography, spectroscopic (IR and UV-visible), thermal gravimetric, magnetization, and magnetic susceptibility measurements. The ESI† also describes antibacterial activity experiments. Below, we have discussed the steps for the preparation of the complex.

2.1 Preparation of the $(CH_3)_2NH_2[Fe(phen)Cl_4]$ complex

The Fe (III)-phenanthroline complex, **1**, was synthesized by combining 1,10-phenanthroline hydrochloride monohydrate with $FeCl_3\cdot 6H_2O$. The experimental process is as follows: a mixture of DMF and HCl in a 5 : 2 (v : v) ratio was used as the solvent. 10 mL of this solvent mixture was taken in a 150 mL reaction flask and 0.145 g (0.802 mmol) of 1,10-phenanthroline hydrochloride monohydrate was added to it. To this mixture, 0.13 g (0.802 mmol) of $FeCl_3\cdot 6H_2O$ dissolved in 8 mL of DMF was added dropwise. A mixture of orange colour was formed and vigorously stirred for 3 hours at 60 °C. This solution was left to slowly evaporate at room temperature. After 3 days, orange prismatic crystals were formed and isolated. The yield of the reaction was 76%. The theoretical contents of C, H, N and Fe in $C_{14}H_{16}Cl_4FeN_3$ were calculated to be 39.7, 3.8, 9.9 and 13.2%, respectively. Experimental elemental analysis showed that the contents of C, H, N and Fe in **1** were 42.6, 3.7, 9.8 and 15%, respectively.

3. Results and discussion

Prior to any characterization and/or physical study, the powder X-ray diffraction (PXRD) experiment on the powder used for measurements (grounded crystals) was performed (Fig. 1). The resultant PXRD patterns for the crystal structure were consistent with the theoretically simulated ones generated from single X-ray diffraction (SXRD) analysis, thus conforming to the phase purity and homogeneity of **1**.

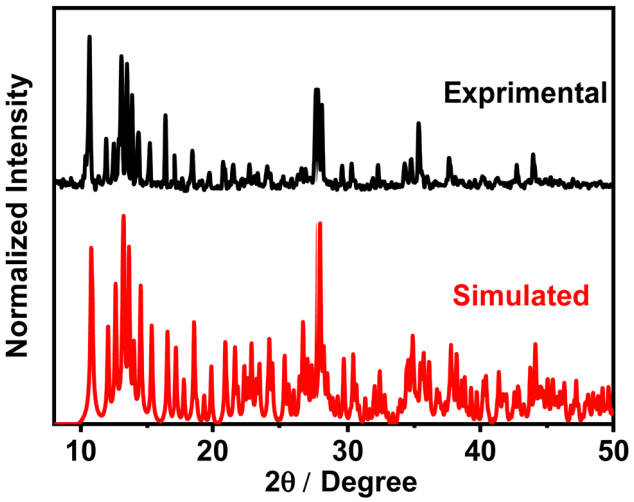

Fig. 1 Experimental (black line) and simulated (red line) X-ray diffraction patterns of $(CH_3)_2NH_2[Fe(phen)Cl_4]$.

Complex **1** dissolves well in water and in polar solutions such as methanol, *N*,*N*-dimethylformamide (DMF) and dimethylsulfoxide (DMSO) forming a yellow-to-orange solution (Fig. S1, ESI†). The complex is stable in air at room temperature.

3.1. Structure description

Fig. 2 illustrates the molecular structure of $(CH_3)_2NH_2[Fe(phen)Cl_4]$, with atom numbering. The structure consists of one 1,10-phenanthroline molecule ligating the Fe(III) ion in a bidentate manner through N atoms, together with four coordinated chlorides and one dimethylammonium cation $(CH_3)_2NH_2^+$. The dimethylammonium cation originates from the decomposition of dimethylformamide solvent as reported in the literature.[49,50]

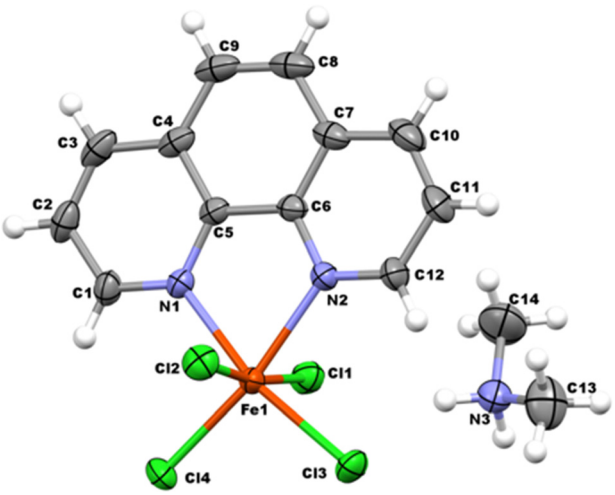

Fig. 2 Molecular structure of **1** with the atom-numbering scheme and 50% probability displacement ellipsoids.

Fe(III) is hexacoordinated and its metal-coordinated-atom (N, Cl) distances and angles in the resulting distorted octahedron are of the same magnitudes as those measured in known complexes (Table S3, ESI†).[47,51,52] Fe–Cl bond distances are quite comparable and vary from 2.3114 (3) to 2.4447 (3) Å. Meanwhile, Fe–N bond lengths are in the range 2.1835 (7)–2.1856 (7) Å. These distances are comparable to those previously reported for hexacoordinated Fe(III) (with two chlorides in equatorial positions, two chlorides in axial positions and two nitrogen atoms from the phenanthroline ligand) in the other iron-based complex.[51,52]

A two-dimensional layered structural system is formed by the interaction between the $[Fe(phen)Cl_4]^-$ anion and the uncoordinated $(CH_3)_2NH_2^+$ cation (Fig. 3). The presence of the free dimethylammonium cation in the complex results in extensive H-bond interactions, which involve both H-atoms bonded to the nitrogen one in the dimethylammonium cation, and a neutral infinite chain nearly parallel with [100] is formed (Fig. 3 and Table 1).

Table 1 represents the values of the geometrical characteristic parameters of H-bonds in the crystal. Two molecules of the complex and two dimethylammonium cations are present in a one-unit cell. The two 1,10-phenanthroline rings bonded to different iron atoms oriented in opposite directions are in different planes. Moreover, a π–π interaction between the ring (C4–C9) and its inversion symmetry located on the adjacent layer consolidates the cohesion of the molecules in the crystal.

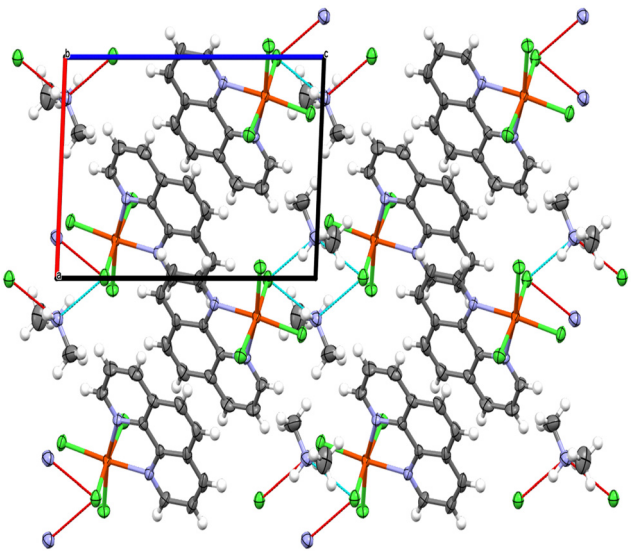

Fig. 3 Packing diagram of **1** along the *b*-axis. Carbon, nitrogen, hydrogen, iron and chlorine atoms are shown in dark grey, blue, white, dark orange and green, respectively, showing intermolecular (dashed lines) N–H···Cl hydrogen bonds.

Table 1 H-bond geometry (distances in Å, angles in °) for **1**

D–H···A	D–H	H···A	D···A	D–H···A
N3–H3A···Cl1i	0.89	2.60	3.2561 (9)	131
N3–H3A···Cl4i	0.89	2.66	3.3435 (10)	135
N3–H3B···Cl1	0.89	2.44	3.2222 (10)	147

Symmetry code: (i) $-x+2, -y+1, -z$.

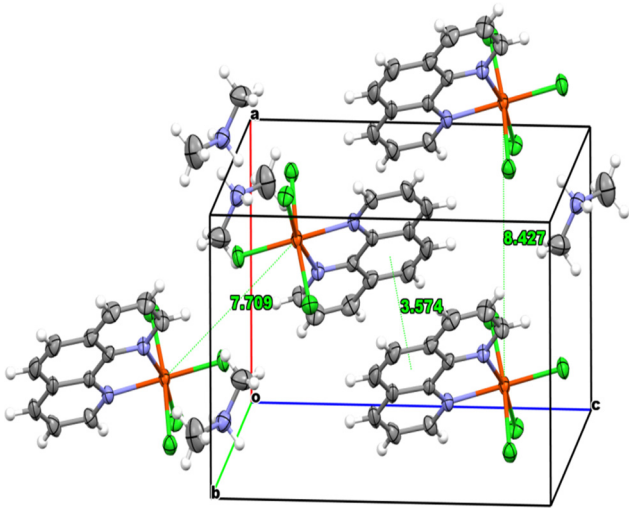

Fig. 4 A three-dimensional view of the structure of **1** showing the stacking of the layers and the distances between the iron atoms.

The distance between their two centroids is 3.5737(7) Å. The 1,10-phenanthroline ring is almost planar with maximum deviation from the mean plan of −0.070(1) Å at C3. Dimethylammonium cations are inserted between the two layers. Fig. 4 shows that the distance between the two iron atoms belonging to the same layer is 7.709 Å, while that between the iron atoms located in the parallel layers stacking along the [100] direction is 8.427 Å.

3.2. Hirshfeld surface

To explore the robustness and its origin in the crystal structure, we studied the interactions in the packing arrangement of the crystal structure. To this end, Hirshfeld surface (HS) analysis[53] was used to visualize and evaluate intermolecular bonds, such as H···H, C···H, Cl···H and Cl···Cl. A wide range of properties can be visualized on the Hirshfeld surface with CrystalExplorer 3.1 program,[54] including the normalized contact distance (d_{norm}) based on the distance of atoms external (d_e) and internal (d_i) to the surface and the van der Waals radii of atoms (r^{vdw}), given by eqn (1), enabling the identification of the regions of particular importance to intermolecular interactions highlighted by red, white, and blue areas.

$$d_{norm} = \frac{(d_i - r_i^{vdw})}{r_i^{vdw}} + \frac{(d_e - r_e^{vdw})}{r_e^{vdw}} \quad (1)$$

where r_i^{vdw} and r_e^{vdw} are the vdw radii of the atoms internal and external to the surface, respectively.

The three-dimensional Hirshfeld surface of $(CH_3)_2NH_2[Fe(phen)Cl_4]$ was generated using CrystalExplorer 3.1. T visualization of the three-dimensional Hirshfeld surfaces prepared by mapping the standard (high) surface resolution d_{norm}, d_e, d_i, curvedness, and shape index on the asymmetric unit of **1** are shown in Fig. 5. The blue patches around the d_{norm} surface are attributed to ring atoms of the molecules inside the surface, and the red ones confirm the presence of non-covalent interactions. These are mainly constituted of N–H···Cl and

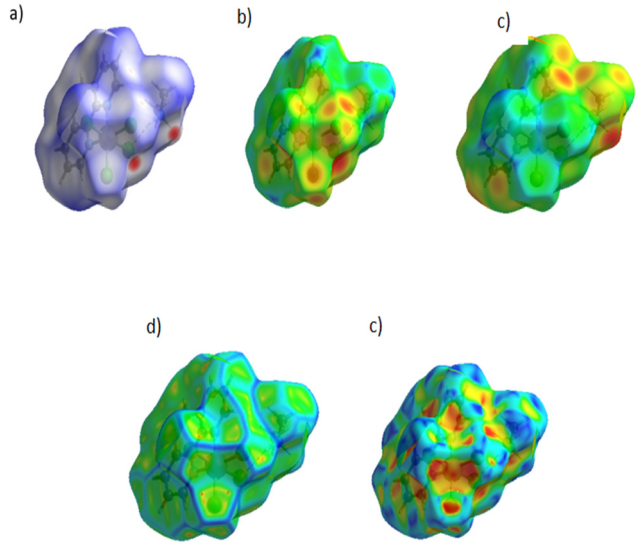

Fig. 5 Hirshfeld surface analysis of $(CH_3)_2NH_2[Fe(phen)Cl_4]$ mapped with: (a) d_{norm}, (b) d_e, (c) d_i, (d) curvedness, and (e) shape-index.

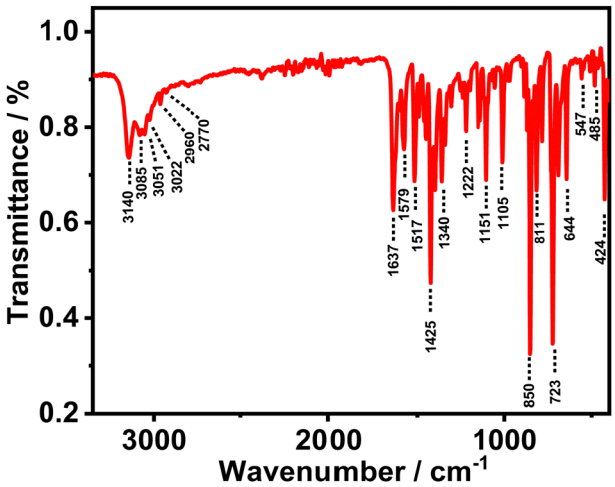

Fig. 6 Infrared spectrum of the $(CH_3)_2NH_2[Fe(phen)Cl_4]$ powder.

correspond to three interactions involving the chlorine atom in the N3–H3A···Cl1^{i}, N3–H3A···Cl4^{i} and N3–H3B···Cl1 H-bonds (Table 1).

The associated fingerprint plots of $(CH_3)_2NH_2[Fe(phen)Cl_4]$ are depicted separately in (Fig. S2(a)–(f), ESI†) showing the contributions of different intermolecular interactions on the Hirshfeld surface. The weak intermolecular interactions in the crystal mainly involve H···Cl and H···H bonds. It is clear that the highest contribution of the total Hirshfeld surface is attributed to the H···Cl/Cl···H bonds (Fig. S2b, ESI†). These appear as two sharp peaks on fingerprint plots with a prominent long peak at $((d_e + d_i) \sim$ 2.5 Å), with a total Hirshfeld surface of 48.3%. There are indeed three N–H···Cl H-bonds in the crystal structure (Table 1). These bonds are electrostatically very favourable due to the partial charges with the opposite charge of chlorine and H atoms. The second most frequent interactions are H···H bonds (Fig. S2c, ESI†) due to the abundance of hydrogen atoms on the molecular surface with no significant effects on the stabilization of the structure. It is important to note that these interactions appear in the middle of the scattered points in the two-dimensional fingerprint map and represent 31.2% of the total HS areas. Furthermore, C···H/H···C bonds (Fig. S2d, ESI†) show the presence of the pair of distinct wings at $((d_e + d_i) \sim$ 2.4 Å) in the 2D fingerprint plot and represent only 11.4%. Other interactions, contribute less to the Hirshfeld surfaces; N···H (1.3%), Cl···Cl (0.3%) and N···C/C···N (0.1%). These results reveal the significance of these interactions in the packing arrangement of the crystal structure.

3.3. Infrared and UV-visible absorption spectra

The powder IR spectrum of **1** exhibits several bands in the region of 450–3200 cm^{-1} (Fig. 6). These bands reflect the vibration transitions of the dimethylammonium cation and 1,10-phenanthroline ligand. In the high frequency domain, the IR spectrum shows broad bands in the 3200–2800 cm^{-1} region, which are attributed to the NH, NH_2, and NH_3 stretching vibrations. The later band centred at 2770 cm^{-1} is due to the CH_2 group stretching. Additionally, the strong bands located in 1637–1618 cm^{-1} and 1517–1425 cm^{-1} regions are assigned to (C═C) and (C═N) stretching vibrations, respectively, of phenanthroline groups.[55,56] The bands at 1517 and 1425 cm^{-1} for the **1** complex are shifted to higher frequencies from their positions for the free 1,10-phenanthroline ligands (1507 and 1420 cm^{-1}), indicating the participation of the nitrogen atom of the phenanthroline ring groups in coordination to the metal ion.[57,58] Moreover, the two peaks located at 848 and 722 cm^{-1} are assigned to ν(C–H) phenyl and pyridine rings, respectively, of the coordinated phenanthroline ligands.[59] Therefore, the band at 424 cm^{-1} could belong to $\nu_{(Fe-N)}$ stretching vibrations. Finally, the bands in the 1250–600 cm^{-1} region are probably due to the C–H in-plane or out-of-plane bend, ring breathing, and ring deformation absorption of 1,10-phenanthroline.

The UV-visible absorption spectra of **1** in different solvents (DMF, MeOH, EtOH and water) were recorded to characterize main transition bands in solutions (Fig. 7). A light-yellow colour of the solutions was seen in EtOH and DMF containing **1**, while an intense yellow to orange colour was seen in MeOH and water solvents. In the spectrum, the n → π* and π → π* charge transfer transitions of the phenanthroline ligand shift from 260–270 nm in the free ligand to 270–280 nm in iron (III) complex ions (285 nm for MeOH and water; and 275–280 nm for EtOH and DMF). The presence of the two absorption bands in the complex at 315–330 nm and 360–370 nm indicates the occurrence of a ligand-to-metal charge transfer event in **1**. The observed shift in the π → π* charge-transfer in this kind of complex has been previously reported and it reflects the coordination of the phenanthroline chelate ligand to the metal iron(III).[41,60] Finally, a very weak absorption band at 508 nm, which can be attributed to weak transitions in the six-coordinated high spin octahedral configuration around the Fe (III) ion, was observed.[28]

3.4. Thermal stability and analysis

Thermal properties of **1** were studied using simultaneous TGA/DTA analyses in the temperature range 20–800 °C in an air

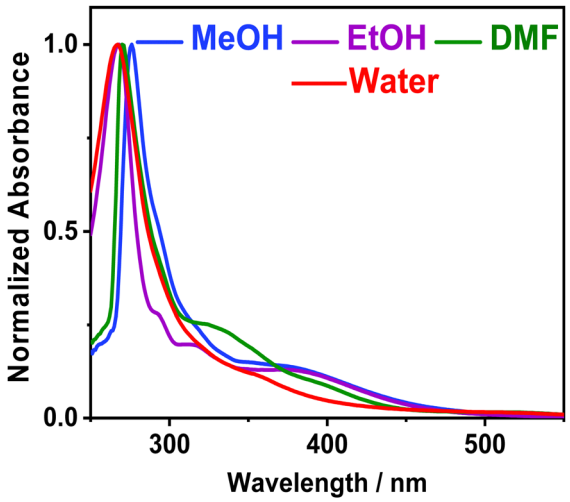

Fig. 7 Normalized UV-visible absorption spectra of $(CH_3)_2NH_2[Fe(phen)Cl_4]$ in different solvents.

atmosphere with a heating rate of 5 °C min^{-1} (Fig. 8). The resultant TGA curve reveals that **1** is stable up to 160 °C, and then, it starts to decompose in three major steps in the temperature ranges 156–280 °C, 280–400 °C and 400–610 °C. The first stage of mass loss occurs in the temperature range 156–280 °C with a drop in the mass by 22.3% (theoretical value, 22.7%), due to the removal of one dimethylammonium cation and one chloride atom per formula unit of the compound. This process is endothermic as it is evident from DTA showing an endothermic peak at 175 °C. At this temperature, the residue corresponds to the mass of [Fe(III)(phen)Cl_3]. The second main stage occurs between 280–575 °C with a total mass loss of 58% (theoretical value, 57.3%), and corresponds to a total loss of one 1,10-phenanthroline molecule and three chloride atoms from the complex, which destroys the main architecture around metal coordination. This phenomenon is coupled with two exothermic events in DTA measurements at 358 and 555 °C.

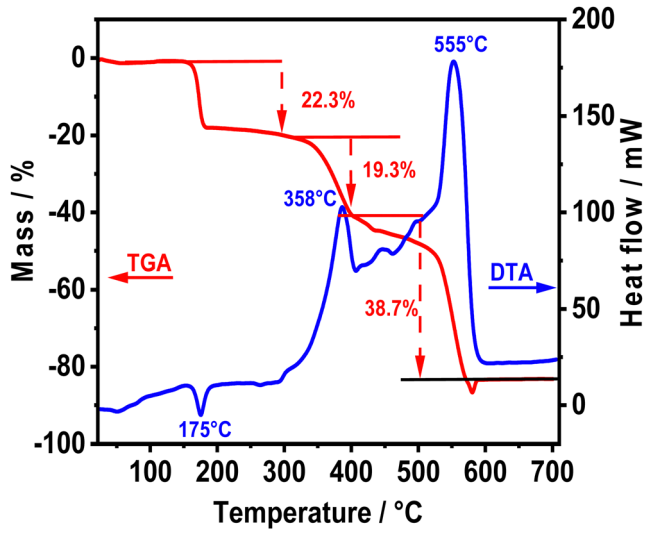

Fig. 8 TGA and DTA behaviours of complex **1**.

The final residue obtained is about 17% and the mass corresponds to the formation of iron (III) oxide $(Fe_2O_3)_{0.5}$ as a residue of thermal degradation. This is in agreement with the previously reported results.[61,62]

3.5. Magnetic properties

To explore the oxidation state of iron in the structure of complex **1**, we carried out temperature-dependent magnetic susceptibility (χ) and magnetisation experiments at temperature ranging from 4 to 300 K on a powdered sample. The plot of χ *vs.* T at different frequencies is shown in Fig. 9(A), the M *vs.* T curve at 100 Oe is shown in Fig. 9(B) and the magnetisation as a function of the magnetic field is presented in Fig. 9(C). From Fig. 9(A)–(C), it is clear that the sample is in a paramagnetic state, which is mainly attributed to the Fe^{3+} ion. The molar magnetic susceptibility $\chi(T)$ does not depend on the frequencies and rises exponentially with decreasing temperature and no features are apparent, demonstrating the lack of magnetic exchange interactions in the complex, which is consistent with an isolated mononuclear complex. $\chi(T)$ shows reasonable agreement with the Curie–Weiss law above 150 K. The calculated effective magnetic moment (μ_{eff}) is given by the formula presented in eqn (2):

$$\left(\frac{\mu_{eff}}{\mu_B}\right)^2 = \frac{3k_B C}{N} \quad (2)$$

where k_B is the Boltzmann constant, C is the Curie constant, N is Avogadro's number and μ_B is the Bohr magneton. The effective magnetic moment (μ_{eff}) directly relates to the number of spins, which is given by eqn (3):

$$\mu_{eff} = g[S(S+1)]^{1/2}\mu_B \quad (3)$$

The obtained experimental value of μ_{eff} (6.1 μ_B) is found to be slightly higher than the theoretical spin-only value for Fe^{3+} (5.92 μ_B). This is in line with other similar research on six-coordinated iron(III) systems and consistent with the presence of five unpaired electrons.[63] Thus, the paramagnetic nature of the compound at 150 K also confirms the Fe^{3+} oxidation state in the $(CH_3)_2NH_2[Fe(phen)Cl_4]$ complex.

3.6. Antibacterial activity assay

The antibacterial activity of **1** was evaluated against two Gram-positive bacteria, *S. aureus* CECT 86 and *L. monocytogenes* CECT 4031, and two Gram-negative bacteria, *E. coli* CECT 99 and *K. pneumoniae* CECT 143T, using the disc diffusion method. Discs of two commercial antibiotics, ciprofloxacin (5 μg) and chloramphenicol (30 μg), were used as a control to compare the antibacterial activity of the synthesized complex (Fig. S3, ESI†). Table 2 shows the mean values of the diameter of the inhibition zone.

It is clear that the values of the diameter of the inhibition zone for **1** are higher for Gram-negative bacteria. The comparison of the values obtained with complex **1** discs with those obtained with ciprofloxacin and chloramphenicol discs shows that complex **1** has lower antimicrobial activity against all the

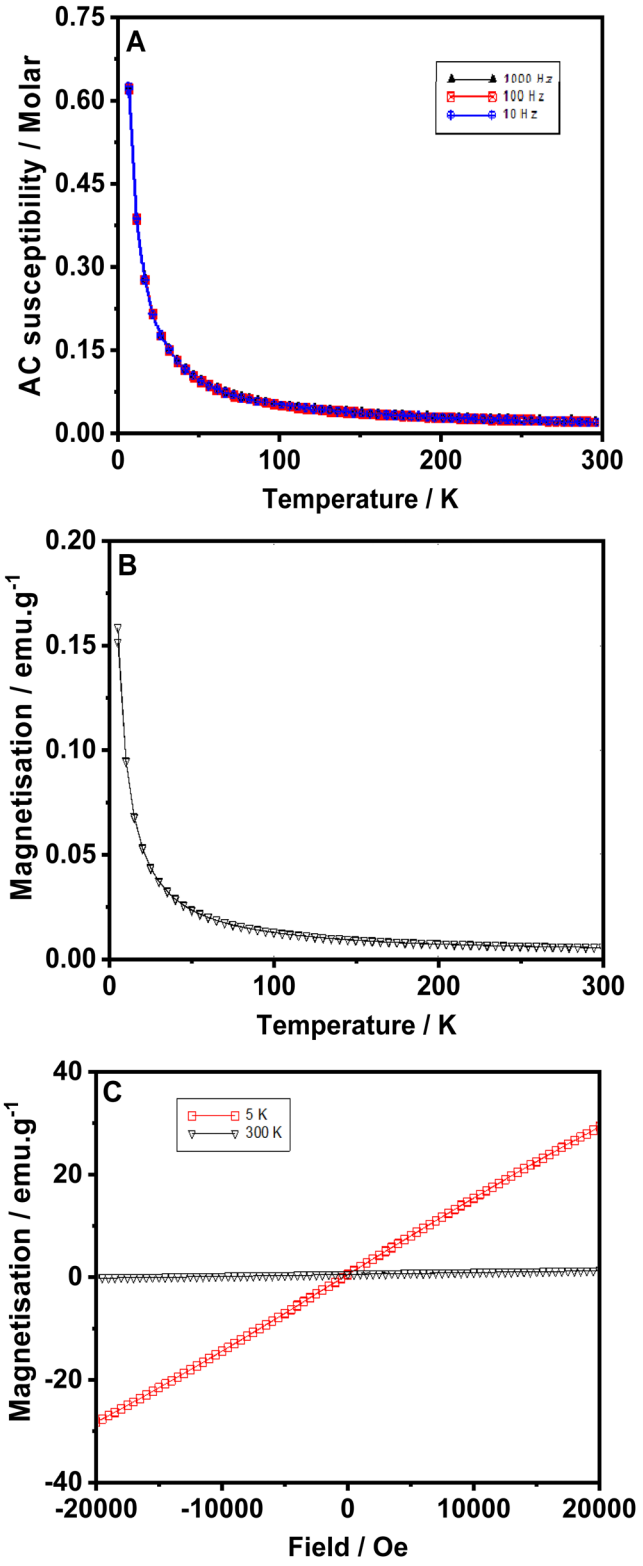

Fig. 9 (A) Temperature-dependence of the magnetic susceptibility of **1** at 10 Hz (blue), 100 Hz (red) and 1000 Hz (black). (B) Magnetization of **1** as a function of temperature at 100 Oe. (C) Plot of magnetization as a function of the magnetic field of **1** measured at 5 and 300 K.

four bacteria assayed using the two drugs except for *L. monocytogenes* tested using ciprofloxacin, for which no inhibition zone was observed. This interestingly indicates that this bacterium is resistant to this antibiotic but sensitive to complex **1**.

Results from the assay to determine the MIC of complex **1** indicate that it was able to inhibit the growth of each of the four bacteria, as shown in Fig. 10. Remarkably, **1** exhibits antibacterial activity against both Gram-positive and Gram-negative bacteria, with some differences in the activities. As shown in Fig. 10, all the assayed concentrations were able to inhibit the growth of the bacteria, at least partially, and the decrease of growth increases with the concentration of **1**. However, for *L. monocytogenes* CECT 4031, the percentage of decrease varies between 78.4% and 89.4% for 300 and 1000 μg mL^{-1}, respectively; for *E. coli* CECT 99, it varies between 17.3% and 93.8% (Fig. S4, ESI†). Based on these results, **1** could be used even to the lowest concentration assayed to inhibit *L. monocytogenes* CECT 4031 growth. For *S. aureus* CECT 86, we observed that using concentrations of **1** higher than 800 μg mL^{-1} did not produce a significant increase in the inhibition of growth, reaching a value of 95.7%. Values for *K. pneumoniae* CECT 143T were the lowest with a decrease of growth of 61.6% at the highest concentration of complex **1** assayed (1000 μg mL^{-1}). This value is very far from that of the MIC, and a higher concentration of **1** would be necessary to reach 100% inhibition of growth. At higher concentrations of **1**, the percentages of decrease of growth are slightly more effective against *S. aureus*, followed by *E. coli* and *L. monocytogenes.*

Two iron(III) complexes, $[Fe(L_1)(L_2)(H_2O)]Cl_3$ and $[Fe(L_1)(L_2)(L_3)(H_2O)]Cl_3$ where L_1 = 1,10-phenanthroline ($C_{12}H_8N_2$), L_2 = 2,2′-bipyridine ($C_{10}H_8N_2$) and L_3 = acetamide (C_2H_5NO), completely inhibited the growth of both the Gram-positive and Gram-negative bacteria at lower concentrations.[64]

A comparative study of these results with Fe(II) complexes reported in the literature reveals that Fe(II) complexes with acyclic chelating ligands show low or virtually no antibacterial activity against the tested Gram-negative and Gram-positive bacteria.[9,65,66]

The reason for the difference in the effectiveness of the tested complexes can be related to the differences in the degree of penetration and interference of the sample with the bacterial cell wall. This is based on different factors such as cell membrane and cell permeability, and such discrepancies in the activities of various strains of bacteria might be due to the difference in the complexity of the cell wall structure of these bacterial strains the effect of the iron (III) ion on normal cell processes as explained by Tweedy's chelation theory[67] and the overtone concept.[68]

4. Conclusion

To conclude, a new iron (III) complex with 1,10-phenanthroline $(CH_3)_2NH_2[Fe(phen)Cl_4]$ was synthesized and fully characterized using different techniques. The single-crystal X-ray diffraction pattern showed that the iron (III) ion is present in a

Table 2 Mean values (n = 2) of the diameter of the inhibition zone (mm) obtained in the assays using $(CH_3)_2NH_2[Fe(phen)Cl_4]$ and two commercial antibiotics to inhibit the growth of the assayed bacteria

	Inhibition zone diameter/mm			
	S. aureus CECT 86	*L. monocytogenes* CECT 4031	*E. coli* CECT 99	*K. pneumoniae* CECT 143T
Disc diffusion method	14.5	15.5	17.0	17.5
Ciprofloxacin disc (5 μg)	26.5	No halo	28.0	27.3
Chloramphenicol disc (30 μg)	20	19.5	19.3	18.8

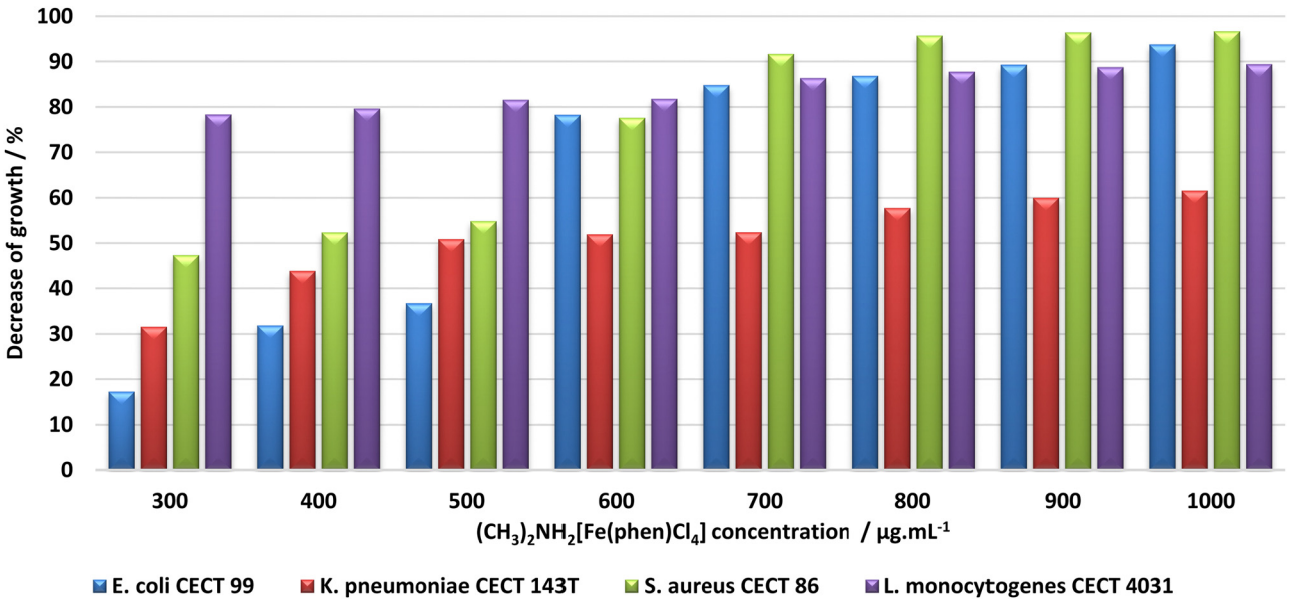

Fig. 10 *In vitro* antimicrobial activity of $(CH_3)_2NH_2[Fe(phen)Cl_4]$ against two Gram-negative and two Gram-positive bacteria.

distorted octahedral geometry coordinating with two nitrogen atoms of the bidentate chelating phenanthroline ligand and four chlorides, with dimethylammonium being present in a cationic form. The complex was characterized using spectroscopic methods (FT-IR and UV-visible) and thermogravimetric analysis. The IR spectrum of the complex is consistent with the bonding of 1,10-phenanthroline to the iron center. The UV-visible absorption spectra in organic and water solvents corroborate the octahedral geometry of the synthesized complex. The temperature-dependent magnetic susceptibility investigations confirmed the Fe(III) state in the $(CH_3)_2NH_2[Fe(phen)Cl_4]$ complex. The results of the *in vitro* antibacterial activity studies against Gram-positive *S. aureus* CECT 86 and *L. monocytogenes* CECT 4031 and Gram-negative *E. coli* CECT 99 and *K. pneumoniae* CECT 143T bacteria demonstrated interesting antibacterial activity of complex **1** against both types of the studied bacterial strains at high concentrations. Thus, our findings suggest that this new Fe(III)/1,10-phenanthroline complex is a good candidate for developing and investigating new iron (III)-based inorganic materials for biological applications.

Conflicts of interest

There are no conflicts of interest to declare.

Acknowledgements

We thank the technical assistance of the Interface Regional University Center at the University Sidi Mohammed Ben Abdellah (USMBA, Fez, Morocco), and the USMBA for financial support. This work is also supported by the following grants: PID2020-116519RB-I00 funded by MCIN/AEI/10.13039/501100011033 and the European Union (EU); SBPLY/19/180501/000212 funded by JCCM (Spain) and the EU through "Fondo Europeo de Desarollo Regional" (FEDER) and 2022-GRIN-343259 funded by UCLM (FEDER). We would like to thank Dr Urbano Diaz (ITQ, CISC-UPV, Valencia, Spain) for carrying out the elemental analysis experiments. We thank Prof. María de los Llanos Palop Herreros (UCLM) for her help in designing and discussing the antibacterial activity experiments and the related results. A. B. A. thanks the grant from the Spanish Service for the Internationalization of Education (SEPIE) for her stay at the UCLM, through the EU Erasmus+ key action program (2020-1-ES01-KA107-079868). S.R.S. thanks the UCLM for her PhD Fellowship (2019-PREDUCLM-10801).

References

1 C. L. Ventola, *P T*, 2015, **40**, 277–283.
2 L. Serwecińska, *Water*, 2020, **12**, 3313.

3 F. Prestinaci, P. Pezzotti and A. Pantosti, *Pathog. Glob. Health*, 2015, **109**, 309–318.
4 G. Annunziato, *Int. J. Mol. Sci.*, 2019, **20**, 5844.
5 D. Chinemerem Nwobodo, M. C. Ugwu, C. Oliseloke Anie, M. T. S. Al-Ouqaili, J. Chinedu Ikem, U. Victor Chigozie and M. Saki, *J. Clin. Lab. Anal.*, 2022, **36**, e24655.
6 A. Frei, *Antibiotics*, 2020, **9**, 90.
7 G. Watanabe, H. Sekiya, E. Tamai, R. Saijo, H. Uno, S. Mori, T. Tanaka, J. Maki and M. Kawase, *Chem. Pharm. Bull.*, 2018, **66**, 732–740.
8 F. X. L. J. Qin, L. Xue, N. Lei, Q. L. Ren, D. Y. Wang and H. L. Zhu, *Acta Chim. Slov.*, 2014, **61**, 170–176.
9 A. Ekennia, A. Osowole and A. Ozukwe, *RRJChem*, 2014, **3**, 32.
10 E. A. M. Khalil and G. G. Mohamed, *J. Mol. Struct.*, 2022, **1249**, 131612.
11 M. Yadav, D. Yadav, D. Pal Singh and J. Kumar Kapoor, *Inorg. Chim. Acta*, 2023, **546**, 121300.
12 V. Uivarosi, *Molecules*, 2013, **18**, 11153–11197.
13 A. Evans and K. A. Kavanagh, *J. Med. Microbiol.*, 2021, **70**, 001363.
14 M. Kumar, K. Kaur Sodhi, P. Singh, P. Kumar Agrawal and D. Kumar Singh, *J. Environ. Nanotechnol.*, 2019, **11**, 100209.
15 I. Elaaraj, S. E. R. Raouan, A. Nakkabi, B. Es-sounni, I. Koraichi, N. El moualij and M. Fahim, *J. Indian Chem. Soc.*, 2022, **99**, 100404.
16 F. Calderazzo, G. Pampaloni and V. Passarelli, *Inorg. Chim. Acta*, 2002, **330**, 136–142.
17 K. Larsson and L. Öhrström, *Inorg. Chim. Acta*, 2004, **357**, 657–664.
18 P. Lenaerts, A. Storms, J. Mullens, J. D'Haen, C. Görller-Walrand, K. Binnemans and K. Driesen, *Chem. Mater.*, 2005, **17**, 5194–5201.
19 I. Kani, O. Büyükgüngör and F. Şişman, *Z. Naturforsch.*, 2006, **61**, 1198–1204.
20 K. Arun Kumar, A. Dayalan and K. Sethusankar, *Acta Crystallogr., Sect. E: Struct. Rep. Online*, 2009, **65**, m1300–1301.
21 I. Kani, Ö. Atlier and K. GüVen, *J. Chem. Sci.*, 2016, **128**, 523–536.
22 A. Kassa, A. Abebe and M. Amare, *Electrochim. Acta*, 2021, **384**, 138402.
23 K. Manna, T. Zhang, F. X. Greene and W. Lin, *J. Am. Chem. Soc.*, 2015, **137**, 2665–2673.
24 J. G. Wang, H. X. Kang and X. Y. Zheng, *Z. Kristallogr. – New Cryst. Struct.*, 2005, **220**, 597–598.
25 X. Tai, N. Wei and D. Wang, *Materials*, 2012, **5**, 558–565.
26 A. Y. Kovalevsky, M. Gembicky and P. Coppens, *Inorg. Chem.*, 2004, **43**, 8282–8289.
27 Z. A. Siddique, Y. Yamamoto, T. Ohno and K. Nozaki, *Inorg. Chem.*, 2003, **42**, 6366–6378.
28 J. Abdelhak, S. Namouchi Cherni, M. Amami, M. Zid and A. Driss, *J. Supercond. Novel Magn.*, 2014, **27**, 1693.
29 V. Amani, R. Alizadeh and A. Khosrojerdy, *J. Struct. Chem.*, 2018, **59**, 1944–1951.
30 Y. Prashanthi, K. Kiranmai, I. Bhatnagar, S. Kumar, V. Chityala and Shivaraj, *Bioinorg. Chem. Appl.*, 2012, **2012**, 948534.
31 H. Camren, M.-Y. Chang, L. Zeng and M. E. McGuire, *Synth. Commun.*, 1996, **26**, 1247–1252.
32 N. Demirhan, I. Erden and U. Avcıata, *Synth. React. Inorg. Met.-Org. Chem.*, 2002, **32**, 1361–1372.
33 A. M. S. Garas and R. S. Vagg, *J. Heterocycl. Chem.*, 2000, **37**, 151–158.
34 N. Lihi, A. J. Godó, G. Sciortino, E. Garribba and K. Várnagy, *Polyhedron*, 2017, **123**, 192–205.
35 J. Chen and W. R. Browne, *Coord. Chem. Rev.*, 2018, **374**, 15–35.
36 T. J. Greenfield, M. M. Turnbull, J. Zubieta and R. P. Doyle, *Inorg. Chim. Acta*, 2019, **498**, 119084.
37 L. Malacaria, G. A. Corrente, A. Beneduci, E. Furia, T. Marino and G. Mazzone, *Molecules*, 2021, **26**, 2603.
38 G. A. Sundaram, K. Vaithinathan and K. Anbalagan, *J. Mol. Struct.*, 2021, **1225**, 129160.
39 W. T. Eckenhoff, A. B. Biernesser and T. Pintauer, *Inorg. Chim. Acta*, 2012, **382**, 84–95.
40 C. P. Matos, Z. Adiguzel, Y. Yildizhan, B. Cevatemre, T. Bagci-Onder, O. Cevik, P. Nunes, L. P. Ferreira, M. D. Carvalho, D. L. Campos, F. R. Pavan, J. C. Pessoa, M. H. Garcia, A. I. Tomaz, I. Correia and C. Acilan, *Data Brief*, 2019, **27**, 104548.
41 S. Tosonian, C. J. Ruiz, A. Rios, E. Frias and J. F. Eichler, *Open J. Inorg. Chem.*, 2013, **3**, 7–13.
42 S. Kaneko, R. Mitsuhashi, M. Mikuriya and H. Sakiyama, *X-Ray Struct. Anal. Online*, 2018, **34**, 49–50.
43 P. Kulkarni, S. Padhye and E. Sinn, *Polyhedron*, 1998, **17**, 2623–2626.
44 H. R. Khavasi, V. Amani and N. Safari, *Z. Kristallogr. – New Cryst. Struct.*, 2007, **222**, 155–156.
45 H. M. Abdel-Halim, A. S. Abu-Surrah and H. M. Baker, *Z. Naturforsch., B: J. Chem. Sci.*, 2006, **61**, 1346–1350.
46 P. C. Healy, J. M. Patrick, B. W. Skelton and A. H. White, *Aust. J. Chem.*, 1983, **36**, 2031–2041.
47 V. Amani, N. Safari, H. R. Khavasi and P. Mirzaei, *Polyhedron*, 2007, **26**, 4908–4914.
48 Y. Huang, M.-E. Moret, B. Klein Gebbink and M. Lutz, *Eur. J. Inorg. Chem.*, 2013, 2467–2469.
49 G. S. Papaefstathiou, S. Manessi, C. P. Raptopoulou, E. J. Behrman and T. F. Zafiropoulos, *Inorg. Chem. Commun.*, 2004, **7**, 69–72.
50 M. Tsuchimoto, N. Yoshioka and S. Ohba, *Eur. J. Inorg. Chem.*, 2001, 1045–1049.
51 H. R. Khavasi, V. Amani and N. Safari, *Z. Kristallogr. – New Cryst. Struct.*, 2008, **223**, 41–42.
52 V. Amani, N. Safari and B. Notash, *J. Iran. Chem. Soc.*, 2013, **10**, 751–761.
53 M. A. Spackman and D. Jayatilaka, *CrystEngComm*, 2009, **11**, 19–32.
54 P. R. Spackman, M. J. Turner, J. J. McKinnon, S. K. Wolff, D. J. Grimwood, D. Jayatilaka and M. A. Spackman, *J. Appl. Crystallogr.*, 2021, **54**, 1006–1011.
55 M. Liang, W.-Z. Wang, Z.-Q. Liu, D.-Z. Liao, Z.-H. Jiang, S.-P. Yan and P. Cheng, *J. Coord. Chem.*, 2003, **56**, 1473–1480.
56 T. P. Gerasimova and S. A. Katsyuba, *Dalton Trans.*, 2013, **42**, 1787–1797.
57 Ö. Tamer, D. Avcı and Y. Atalay, *J. Inorg. Organomet. Polym. Mater.*, 2017, **27**, 700–713.

58 M. Aslantaş, E. Kendi, N. Demir, A. E. Sabik, M. Tümer and M. Kertmen, *Spectrochim. Acta, Part A*, 2009, **74**, 617–624.
59 R. Křikavová, J. Vančo, Z. Trávníček, R. Buchtík and Z. Dvořák, *RSC Adv.*, 2016, **6**, 3899–3909.
60 J. Simaan, S. Poussereau, G. Blondin, J.-J. Girerd, D. Defaye, C. Philouze, J. Guilhem and L. Tchertanov, *Inorg. Chim. Acta*, 2000, **299**, 221–230.
61 A. De, D. Dey, A. Das, N. Kole and B. Biswas, *Chem. Sci. J.*, 2018, **130**, 26.
62 X. Hu, J. Guo, Y. Wang and C. Liu, *Spectrochim. Acta, Part A*, 2009, **74**, 48–51.
63 P. B. Pansuriya and M. N. Patel, *J. Enzyme Inhib. Med. Chem.*, 2008, **23**, 230–239.
64 G. Tamiru, M. Abiye, A. Melese and A. Abebe, *Chem. Biol. Drug Des.*, 2021, **101**, 479–488.
65 A. Lawal, A. S. Shodeinde, S. A. Amolegbe, S. E. Elaigwu and M. T. Yunus-Issa, *J. Appl. Sci. Environ. Manage.*, 2017, **21**, 568–573.
66 S. N. Abdoon, S. S. M. Al-Obaidy and Y. F. Al-Khafaji, *Res. J. Pharm., Biol. Chem. Sci.*, 2022, **5**, 1231–1241.
67 B. Tweedy, *Open J. Inorg. Chem.*, 1964, **55**, 910–918.
68 Y. Anjaneyulu and R. P. Rao, *Synth. React. Inorg. Met.-Org. Chem.*, 1986, **16**, 257–272.